Physical parameters associated with the dielectric breakdown of MgO crystals at high temperatures

K. L. Tsang and Y. Chen
Solid State Division, Oak Ridge National Laboratory, Oak Ridge, Tennessee 37830

H. T. Tohver
Department of Physics, University of Alabama, Birmingham, Alabama 35294
(Received 27 December 1983)

The dielectric breakdown of MgO crystals at elevated temperatures is investigated as a function of such parameters as temperature, thickness, electric field, ambient atmosphere, electrode material, and impurity content. The prebreakdown electrical characteristics induced by these parameters are studied. Each parameter is investigated individually. The results are found to be compatible with the double injection model.

I. INTRODUCTION

Refractory materials are important in the application of advanced energy technology, such as the magnetohydrodynamic generator. However, material degradation, such as dielectric breakdown, is a serious problem in the application of these materials at high temperatures in electric fields. Therefore, the study of the dielectric breakdown of refractory materials at high temperatures is technologically important. The mechanisms involved no doubt depend on the material and the conditions under which breakdown occurs. The dielectric breakdown of materials is associated with many physical parameters, such as temperature, geometry, electric field, ambient atmosphere, electrode material, and impurity, and therefore is a complicated phenomenon. In order to better understand the nature of the breakdown, one should be able to identify the effect of the various parameters on the breakdown. In this work, we study a system in which the electrical properties change slowly and ultimately trigger a breakdown.

Past investigations focused primarily on breakdown strength[1–14] rather than the breakdown process. The breakdown strength is the maximum electric field strength a material can withstand before it breaks down (in ms or less). Several theoretical models have been proposed for dielectric breakdown,[15–26] but none can satisfactorily account for the phenomena of concern here.[27,28] Recently, the prebreakdown behavior of MgO crystals was studied at high temperatures,[27–33] and it was found that prebreakdown phenomena revealed direct information about the breakdown process. From this information a breakdown mechanism involving double carrier injection attended by migration of negatively charged ions or vacancies was deduced.[27,28] In this paper we extend the study of the dielectric breakdown of MgO crystals at high temperatures to include the effects of the important physical parameters described above.

II. EXPERIMENTAL PROCEDURES

Crystals used in this work were grown at the Oak Ridge National Laboratory (ORNL) and Tateho Chemical Company. The ORNL crystals, doped and undoped, were grown by the arc-fusion method[34] using high-purity MgO powder from Kanto Chemical Company, Tokyo, Japan. Crystals doped with H, Co, Cu, Fe, Ni, Cr, or V were used. The concentration of dopants was determined by neutron-activation analysis and was reported previously.[29]

The sample dimensions were chosen such that the surface distance between electrodes was much greater than the thickness and, therefore, the effect of surface conduction was minimized. Two types of measurements were carried out, current and potential profiles. For current measurements, samples of dimensions $15\times15\times2.5$ mm^3 were used, except when thickness dependence was investigated and when high electric fields were used. Samples were prepared by cleaving along (100) planes and abrading on SiC papers. The abraded surfaces were then removed by chemical polishing in hot phosphoric acid.

For measurements of the potential profile along the thickness of the sample, thick samples were used in order to obtain several data points between the electrodes. Therefore, the sample had to be specially prepared in such a way that the problem of surface conduction could be minimized and the potential at a given point could be correctly measured without disturbing the electric field. The sample-electrode configuration for the potential-profile measurement is shown in Fig. 1. A rectangular block of MgO:Ni single crystal with dimensions $10\times10\times5.6$ mm^3 was cut by a diamond wafering blade (0.2 mm thick) at five positions between two (100) planes to which the electrodes were attached. During the cutting, both the crystal and the diamond blade were rotating at the same time so that the crystal was cut in the desired shape. After cutting, the sample had a central cylindrical solid 6.2 mm in diameter and six extended bladelike projections. It was then chemically polished in phosphoric acid at 330 K for several hours to remove the damaged surface layers. Five individual platinum wires serving as probes were then wrapped around the central cylindrical solid.

The experimental setup has been described previously.[27] In brief, the sample was sandwiched between two flat cir-

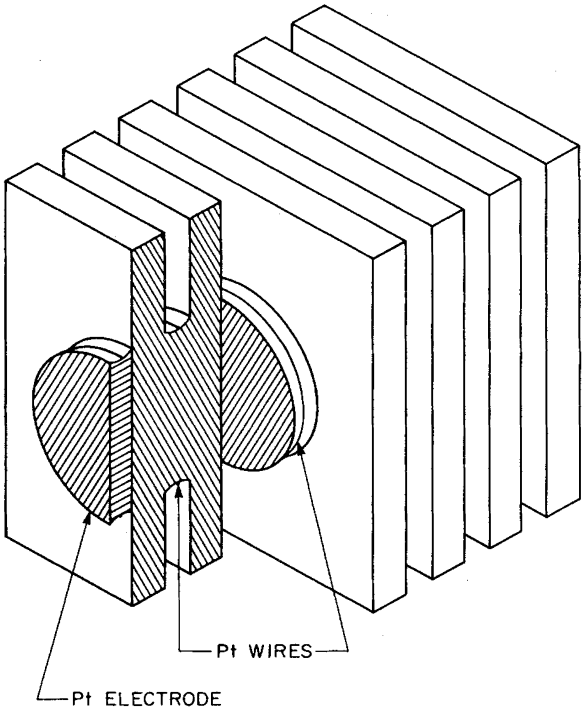

FIG. 1. Diagram of sample configuration for the measurement of potential profiles.

cular platinum electrodes with a diameter of 6.3 mm, and then suspended in the hot zone of a vertical alumina furnace tube which had one hole on each end to allow circulation of the desired atmosphere. A Sentry 7AV electric furnace was used. The furnace temperature was regulated by a Wheelco temperature controller. The temperature was monitored by Pt/Pt (10 at. % Rh) thermocouples and did not fluctuate by more than ±2 K. Unless otherwise noted, platinum electrodes were used and the samples were sustained in air. Both constant and alternating fields were used. For current measurements, a power supply and current recorder were connected in series with the sample. For potential-profile measurements, a potential divider with a total resistance of $10^9\ \Omega$ and a ratio of 1000:1 was connected in parallel with the electrodes to measure directly the value of the potential at various points inside the sample. All measurements were made by a two-probe method since surface conduction was found to be negligible.[27] The experimental procedures were designed to study each parameter individually. Measurements were focused on the prebreakdown behavior, which provides direct information of the breakdown process.

III. RESULTS AND DISCUSSION

A. General features

The general current features were similar for all the MgO crystals investigated. Experiments on MgO:Ni (4000 ppm) crystals are described in this section to illustrate the general behavior of the current response.

1. Current behavior with field reversal

When a moderate dc electric field was applied to a MgO crystal at elevated temperatures, a slight decrease in current was observed initially. Subsequently, the current increased exponentially until the sample experienced dielectric breakdown and could no longer be used as an electrical insulator. Experimentally, the sample was not allowed to proceed to breakdown since this would have destroyed it. When the current reached 18 mA the applied field was removed (or reversed), because at this current the breakdown was imminent and the sample temperature began to significantly exceed the ambient temperature.[27] Therefore, the time required for the current to reach 18 mA was considered to be the characteristic time for breakdown, t_c. Usually, several field reversals were made. The current behavior of a MgO:Ni sample is shown in some detail in Fig. 2.

A field of 1500 V/cm was applied at $t=0$, after the sample had been annealed at 1473 K for about 10 min in order to assure that the sample temperature had reached equilibrium. The current initially decreased from 0.20 to 0.10 mA in 30 min (top, inset, Fig. 2), and then increased exponentially until 18 mA was reached, corresponding to $t=16$ h. This value , 18 mA, represents a 180-fold increase from the minimum current value. Upon field reversal, the current flowing in the opposite direction decreased from an initial value, which was about −18 mA, to a minimum value of −0.7 mA in 25 min (bottom, inset, Fig. 2), and then increased exponentially at a rate faster than that in the first cycle. The characteristic time for breakdown in this cycle was only 10 h. Several more field reversals were subsequently performed. The current behavior was similar to that of the first reversal, but the characteristic time diminished with each reversal, until ultimately only 1.5 h were required. Figure 3 is a plot of the characteristic time for breakdown as a function of chronological field reversals. The decreasing time trend is evident. Five other MgO:Ni crystals were studied in a similar fashion. The results were similar to those shown in Figs. 2 and 3, although the experimental values differed slightly.

The time-dependent current for each of the reversals

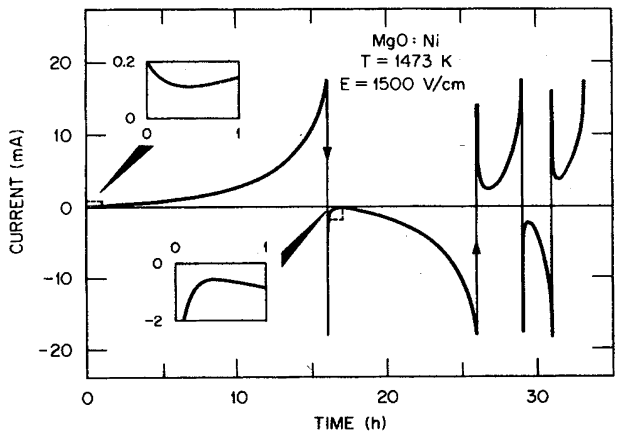

FIG. 2. Current vs time at 1473 K with $E=1500$ V/cm applied to a MgO:Ni crystal for several polarity reversals.

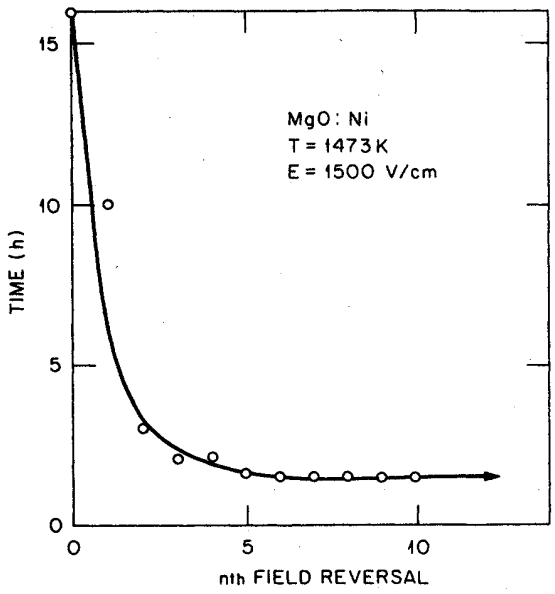

FIG. 3. Characteristic time for breakdown vs the nth field reversal.

can be described accurately as the sum of two exponentials,

$$I(t)=I_{01}e^{-t/\tau_1}+I_{02}e^{t/\tau_2} \text{ for } t>0\,, \quad (1)$$

where I_{01}, I_{02}, τ_1, and τ_2 are positive constants, and $I_{01}>I_{02}$, and $\tau_1<\tau_2$. These constants are obtained from the values of $I(t)$ plotted on a semilogarithmic scale, as shown in Fig. 4. Equation (1) shows a minimum in $I(t)$ at a time denoted by t_m. At $t<t_m$, the first term, $I_{01}e^{-t/\tau_1}$, is predominant, and therefore the current is decreasing. At $t>t_m$, the second term , $I_{02}e^{t/\tau_2}$, dominates and leads to the breakdown. The values of τ_1 and τ_2 diminished with each field reversal. After the tenth field reversal, τ_1 and τ_2 reached their minimum values. The temperature dependence of these two parameters was then investigated and reported elsewhere.[27]

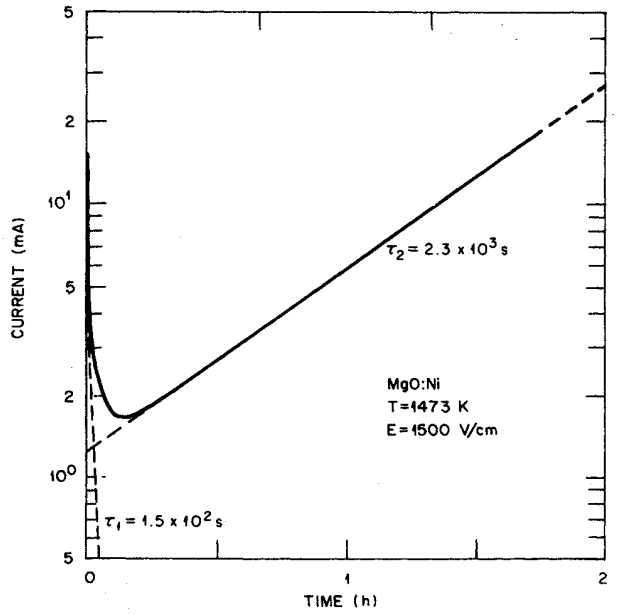

FIG. 4. Log of current vs time. The current was obtained after tenth field reversal. The line associated with τ_1 was obtained by subtracting the line associated with τ_2 from the original curve.

When the applied field was reversed frequently, such as for an alternating field with a frequency of 60 Hz, the current was found to be constant in magnitude after some small fluctuations.[27] Therefore, the alternating electric field did not produce the breakdown, as indicated in Eq. (1). This result and the decreasing behavior of the reversed current led to our conclusion that the dielectric breakdown observed in this study is not initiated by a thermal breakdown mechanism. The reasons are (1) the alternating field should enhance the breakdown because the power loss in a dielectric increases with frequency, and (2) the thermal effect (Joule heating) is independent of the current direction and, therefore, reversing the applied field should not lead to a decrease in current.

2. *Short-circuit current*

Short-circuit current (I_{SC}), which flows from one sample surface to the other via an external conductor when the applied field is removed, can provide information about residual stored charges. It was measured after the applied field had been reversed for different time periods. Figure 5(a) shows five different points along a typical current curve before and after the field reversal. The short-circuit currents measured at these points are shown in the corresponding numbered curves of Fig. 5(b). The positive current direction is defined as the direction of the initial current before the first field reversal. Curve 1 was obtained just before the field reversal, i.e., at $I=+18$ mA.[27] The short-circuit current was about 3 orders of magnitude smaller and flowed in the direction opposite to the original current. It decreased rapidly in the first minute, from an initial value of about 20 μA. Subsequently, the decay became slower. At $t>10$ min, the short-circuit current reached a nearly constant value of about 4 μA. The temperature dependence of the short-circuit current was then studied at $t>10$ min.[27] The results will be described later. Curve 2 was obtained immediately (<1 sec) after the field was reversed. The short-circuit current, initially flowing in the positive

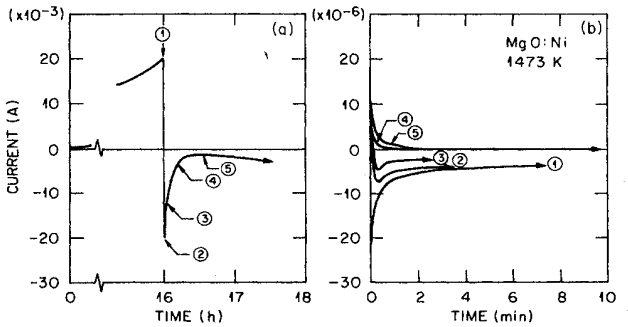

FIG. 5. (a) Five points along a typical current-time curve before and after the field reversal. (b) Short-circuit current vs time. These currents were measured at points shown in (a).

direction, decreased rapidly from about $+2\ \mu A$ to zero in a few seconds, and then flowed in the negative direction. Then the current increased to a maximum (about $8\ \mu A$) before it decreased in a behavior similar to curve 1. Curve 3 was obtained 10 sec after the field was reversed. The current behaved similarly as that shown in curve 2, but the current showed a higher initial positive value and a lower negative saturation value than curve 2. Curve 4 was measured 15 min after the reversal, just before the reversed current reached its minimum. The short-circuit current flowed in the positive direction and decayed to zero in about 1 min. Curve 5 was obtained 30 min after the reversal, when the reversed current was increasing. The current behavior was similar to that in curve 4, but its magnitude was larger.

The short-circuit current flows in a direction opposite to that prior to removal of the electric field. The negative short-circuit current indicates that there are some residual homocharges created by the application of the dc field. These residual charges can be removed or neutralized by field reversal for a time period t_m. These charges are believed to be trapped holes and are directly responsible for the decrease in the reversed current as shown in Eq. (1). From the value t_m and the dimension of the sample, it is estimated that this charge carrier has a mobility of $\sim 10^{-7}\ cm^2/V\ sec$.

3. *Potential profile*

The potential profile of the sample during the application of an electric field can provide information to identify the breakdown mechanisms.[33] The potential profiles of MgO:Ni crystals at 1473 K were measured at different current levels with the field applied, as well as after the removal of the applied voltage. A dc voltage of 560 V was applied to the sample, which had a thickness of 5.6 mm; the electric field strength was therefore 1000 V/cm. The measurements were performed both in the first cycle as well as after the voltage was reversed.

The information provided by the potential profiles is intended to be exploratory. It is desirable to be able to deduce charge densities from these profiles. However, it is not feasible to do so from seven data points. Obtaining these points was already formidable in that it required large single crystals which had to be machined to the shape shown in Fig. 1, often with sample fatalities. The cuts were made deep in order to maximize the surface distance between the wire probes, thereby further compounding the machining difficulties. Nevertheless, the profiles do permit us to draw several relevant conclusions.

a. First cycle. Several sets of potential measurements were performed at various stages before the current reached 18 mA. Each set of measurements is plotted as a numbered curve in Fig. 6. Curve 1 was obtained at $t=0$, immediately after the voltage was applied to the sample. The potential was nonlinear and the data were not symmetric with respect to the center of the crystal. The potential gradient was greatest near the electrodes. Curve 2 was obtained at $t=10$ sec after the application of the voltage when the current was decreasing. The curve is similar to curve 1, except that the central flat region voltage was lower. The voltage drop in the region near the anode was more pronounced. Curve 3 was obtained at $t=19$ min when the current was 0.18 mA and at its minimum point. The potential in the central region increased slightly and the data became more linear. Curve 4 was obtained at $t=2$ h when the current was 0.3 mA and increasing. This curve is similar to curve 3, and the data became even more linear. Subsequently, curves 5, 6, and 7 were measured at $I=0.7$, 9.6, and 17.8 mA, respectively. These three curves are similar and, with increasing time, they more nearly approached linearity.

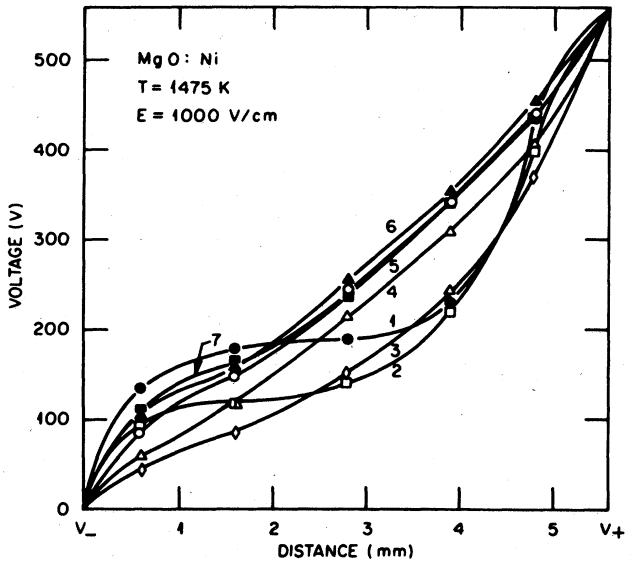

FIG. 6. Potential profiles of MgO:Ni crystal at 1475 K using an electric field of 1000 V/cm. The profiles, as shown in the numbered curves, were measured at various stages during the current increase. The current levels at which the measurements were made are described in the text.

The residual potential profiles were measured at two different current levels at which the applied voltage was removed, as shown in Fig. 7. Data for the top curve were obtained when current was 1.15 mA and increasing. This curve has a negative second derivative in the region close to the cathode and a positive second derivative in the region near the anode. It is indicated that, using the Poisson equation, there are some residual heterocharges, space charges of opposite sign to that of the electrode, in the regions near the electrodes. Data for the lower three curves were measured at 0, 40 sec, and 30 min after the removal of the applied voltage when the current reached 18 mA. The residual voltage in the center region of the crystal became essentially constant shortly after the removal of the applied voltage. It is also noted from Fig. 7 that the initial residual potential difference across the sample, $V(\pm)=2.4$ V at $t=0$, measured from 1.15 mA, and 0.6 V measured from 18 mA.

Several interesting observations are noted from Figs. 6 and 7.

(1) The potential profile (Fig. 6) varies with time and changes from nonlinear (curve 1) to nearer linear (curves 5–7) at higher current levels.

(2) The distribution of the electric field obtained from

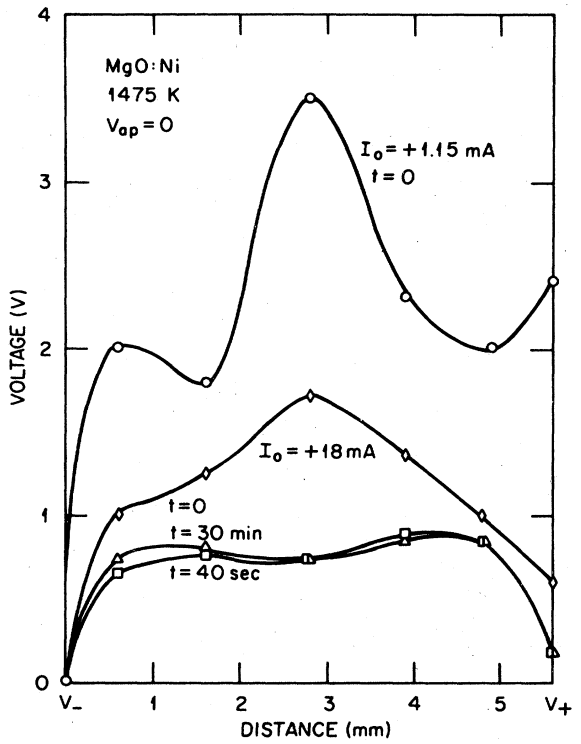

FIG. 7. Residual potential profiles after the removal of the applied field. The top curve was measured when the field was removed at $I=1.15$ mA. The lower three curves were measured at 0, 40 sec, and 30 min after the removal of the field when the current reached 18 mA.

the potential profile also varies with time. Initially, the electric field strength is much higher in the regions near electrodes than in the central part of the crystal. The distribution of the electric field becomes more uniform as the current rises; this indicates that local electrical neutrality prevails as current increases.

(3) Before the current reaches its minimum value, the potential profiles (curves 1—3 in Fig. 6) show that the development of the potential in the region near the cathode is much faster than that near the anode. This rapid buildup of potential indicates that there is a high electron injection as soon as the field is applied to the sample.

(4) The potential profiles indicate that there is no obvious polarization effect during the application of a dc electric field, such as that observed by Moulson *et al.*[35] in aluminous cements and that observed by Cohen in pure alumina.[36] Otherwise, the potential drop in the regions near the electrodes would increase with time, and also the potential profile would become more nonlinear instead of linear. Therefore, the breakdown observed in this study is not initiated by a local breakdown arising from the polarization effect.

(5) The initial residual potential difference across the sample decreases as the current increases (Fig. 7). This fact indicates that the whole sample is approaching the plasma condition[37] (electrical neutrality) as the current increases.

b. After field reversal. Potential profiles were also measured after the applied field was reversed at 18 mA. Several sets of measurements were made and the data are plotted as a respectively numbered curve in Fig. 8. Curve 1 was obtained at $t=0$, immediately after the applied voltage was reversed. The curve showed a nonlinear potential distribution. The potential drop was higher in the region near the new cathode (anode before field reversal) than near the anode. Curve 2, obtained at $t=1$ min when the current was -1.8 mA and decreasing, was similar to curve 1, except that the potential drop near the cathode had increased and that near the anode had decreased. Curve 3, obtained at $t=11$ min when the current was -0.9 mA and decreasing, was similar to curve 2, but the potential drop inside the sample decreased, and hence the potential drop increased in the region near the anode but decreased in the region close to the cathode. Curve 4 was obtained at $t=43$ min when the current was at its minimum (-0.8 mA). The curve is similar to curve 3, but it has a higher potential drop near the anode. Subsequently, curves 5, 6, 7, and 8 were measured at $I=-0.83$, -2.3, -6.8, and -17.2 mA, respectively, while the current increased exponentially. The potential profiles became more linear at higher current levels.

There are several interesting observations which can be noted from the data in Fig. 8.

(1) There are some negative space charges (electrons) left behind from the previous treatment (first cycle) in the region near the new anode (curve 1), and these space charges are easily removed by the reversed field (curve 2), indicating that they are mobile.

(2) Inside the sample there exists an abundance of positive space charges (holes) left behind from the previous treatment, and these space charges are not readily removed by the reversed field (curves 2—4), indicating that they are essentially immobile.

(3) There are probably some negatively charged ionic

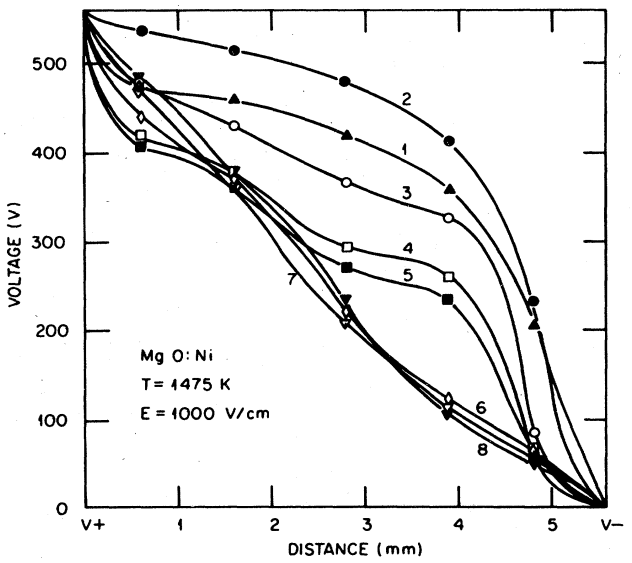

FIG. 8. Potential profiles after the field reversal. The profiles were measured after the field was reversed at $I=18$ mA. The current levels at which measurements were made are described in the text.

species (or vacancies) accumulated in the region very close to the new cathode (curves 1 and 2).

(4) The potential profile becomes more nearly linear as the current increases. This effect is similar to that observed in the first cycle.

B. Temperature effect

The effect of temperature on breakdown was studied by measuring the temperature dependence of the time constant τ_2 of Eq. (1), since τ_2 is directly related to characteristic time for breakdown. At a given field, the value of τ_2 was found to obey the relationship

$$\tau_2=\tau_{02}\exp(Q_2/kT)\ , \tag{2}$$

where the activation energy Q_2 was found to be 2.3 eV for MgO crystals doped with 4000 ppm Ni impurity in the temperature range from 1380 to 1680 K.[27]

C. Effect of sample thickness

The breakdown characteristics of MgO crystals are nearly independent of the sample thickness. Thickness-dependence measurements were performed on MgO:Ni crystals at 1473 K using 1500 V/cm for thickness ranging from 0.2 to 9.1 mm. The time constant τ_2 in Eq. (1) is determined as a function of sample thickness. For a given field, the time constant τ_2 varied between 1.1×10^4 and 0.8×10^4 sec. This thickness independence of breakdown indicates that any migration of the negatively charged ionic species or vacancies is short ranged.

D. Field-strength effect

The investigation of the field-strength effect on breakdown was performed at 1473 K on (i) as-grown MgO:Ni crystals, and (ii) MgO:Ni crystals which had been treated at 1473 K using an electric field of 1500 V/cm for more than 10 field reversals. The results are described in terms of the time constant τ_2 rather than the characteristic time for breakdown, t_c, because the time constant τ_2 is not only directly related to the breakdown time, but it also has a simple relationship with the applied field. The values of τ_2 have been found empirically to decrease exponentially with the applied field strength, as described by

$$\tau_2(E)\propto\exp(-\beta E)\ , \tag{3}$$

where β is a positive constant, and $\beta E>0$. The value of β depends on the history of the sample as well as the applied field.

In the case of the as-grown samples, samples of thickness 2.5 mm were used for field strengths of 200 to 5000 V/cm, and samples of thickness 0.5 mm were used for field strengths of 1.5×10^3 to 3×10^4 V/cm. The value of the log of τ_2 are plotted against thickness in Fig. 9. The value of β was found to be (i) 2.3×10^{-3} cm/V for field strengths from 0.2 to 1 kV/cm, (ii) 5.5×10^{-4} cm/V for field strengths from 1 to 5 kV/cm, and (iii) decreasing with increase of the field. It is estimated that the value of β is of the order of 10^{-5} cm/V when the field strength reaches a magnitude of 10^6 V/cm.

In the case of samples with more than 10 cycles of field-reversal treatments, the value of β was found to be the same (2.7×10^{-3} cm/V) at temperatures of 1473 and 1673 K for field strengths of 1 to 2 kV/cm, as shown in Fig. 10. This value is about 5 times greater than that obtained from the as-grown samples under the same electric field.

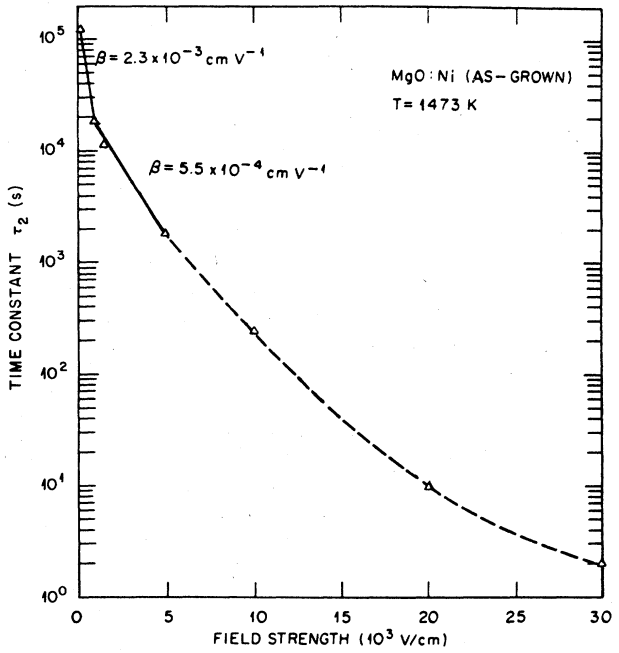

FIG. 9. Log of time constant τ_2 vs electric field strength. The measurements were made on as-grown MgO:Ni crystals.

Taking into account the temperature effect [Eq. (2)], the time constant τ_2 can be expressed as

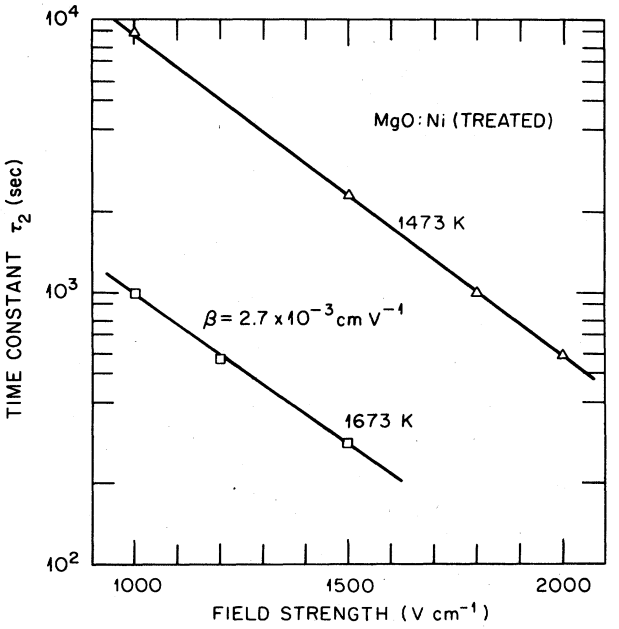

FIG. 10. Log of the time constant τ_2 vs electric field strength. The measurements were performed after the tenth field reversal. Results were obtained at 1473 and 1673 K.

$$\tau_2=\tau_{02}\exp[(Q_2/kT)-\beta E]\ , \quad (4)$$

where Q_2 is activation energy, τ_{02} is a constant for a given electric field range, and β is the constant described above. The pre-exponential constant I_{02} of Eq. (1) is also found to be approximately proportional to the applied field strength. Using Eqs. (1) and (4), and the values of $Q_2=2.3$ eV and $\beta=10^{-5}$ cm/V, one can estimate that the breakdown strength of MgO crystals at $T=700$ K is of the order of 10^6 V/cm, a value which is consistent with the results obtained by Lewis *et al.*[38,39]

E. Ambient atmosphere effect

The dielectric breakdown of MgO:Ni crystals at 1473 K was also examined, using an electric field of 1500 V/cm, in flowing oxygen and nitrogen atmospheres. (The partial pressure of O_2 in a nitrogen atmosphere is about 10^{-4} atm.) The results are shown in Fig. 11. The current behavior was similar in both oxygen and nitrogen atmospheres. In the first hour, the current increased more rapidly in an oxygen or a nitrogen atmosphere than in air. Subsequently, the currents increased exponentially with nearly the same time constant. At high current levels, the rate of current increase was less in air than in either oxygen or nitrogen. The characteristic times for breakdown of MgO crystals at 1473 K in pure oxygen, pure nitrogen, and air were 7.5, 7, and 16 h, respectively. Since air is a composite of these two gases, it is not immediately obvious why the breakdown time in air is twice that in the others.

F. Electrode effect

The observed breakdown characteristics depend strongly on the electrode material. Four kinds of electrode materials were used: platinum, rhodium, iridium, and graphite. Because most of those materials, especially Ir and graphite, are easily oxidized in air at high temperatures,[40,41] all the measurements were performed in a flowing dry-nitrogen atmosphere. Both the cathode and the anode were of the same material.

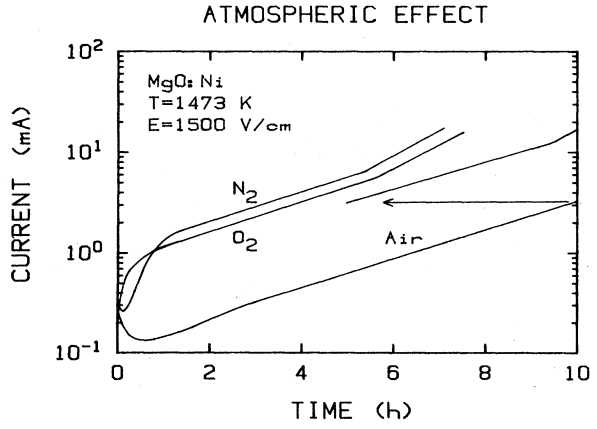

FIG. 11. Effect of atmospheric conditions on the current behavior of MgO:Ni crystals. The log of current is plotted vs time. Three different atmospheres were used: pure oxygen, pure nitrogen, and air.

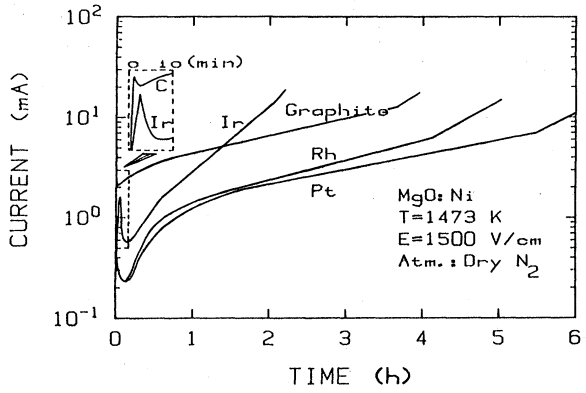

FIG. 12. Effect of electrode material on the current behavior of MgO:Ni crystals. Samples were treated at 1473 K with the use of an electric field of 1500 V/cm in flowing dry N_2. Four different electrodes were investigated: Ir, graphite, Rh, and Pt.

The current behavior and the characteristic times for breakdown of MgO:Ni crystals using different electrodes at 1473 K with an applied field of 1500 V/cm are illustrated in Fig. 12 and Table I. During the first 30 min after the application of the voltage, the current behaved differently for different electrode materials. Graphite and iridium electrodes provided a similar initial current behavior. Both currents increased rapidly to a maximum, and then decreased to a minimum before increasing exponentially. Platinum and rhodium electrodes exhibited a similar current behavior to that described previously (see Fig. 11). After 30 min all four materials displayed an exponential current increase. Samples with Pt, Rh, and graphite electrodes increased with nearly the same time constant. In the case of Ir, the time constant was about 4 times smaller and, therefore, resulted in a shorter breakdown time. The characteristic times for breakdown of the crystals at 1473 K using an electric field of 1500 V/cm in a dry-nitrogen atmosphere were 2, 4, 5, and 7 h for Ir, graphite, Rh, and Pt electrodes, respectively. Different combinations of these electrode materials were also used as cathode and anode. The current behavior described above was found to be determined primarily by the cathode material.

The activation energies obtained from the temperature dependence of the short-circuit current using different electrode materials under the conditions described above are also shown in Table I. The values range from 2.6 to

TABLE I. Characteristic times for breakdown, t_c, and the activation energies, Q, of MgO:Ni crystals using different electrode material. The measurements were performed at 1473 K using an electric field of 1500 V/cm in a flowing dry-nitrogen atmosphere.

Electrode material	t_c (h)	Q (eV) (±0.1)
Ir	2	2.9
Graphite	4	a
Rh	5	2.7
Pt	7	2.6

[a]Note measured (see text).

2.9 (±0.1) eV. Usually, the short-circuit current flows in the direction opposite to the original current and lasts for a long time. However, in the case of graphite electrodes, the short-circuit current, as measured after the field was removed at 18 mA, flowed in the same direction as the original current and decreased from about 3 mA to nearly zero in only 30 sec. Therefore, no activation energy could be determined when using graphite electrodes.

Different electrode materials form different potential barriers at the electrode-oxide interface and, therefore, provide different work functions for the charge carrier to be injected. According to the results described above, Ir electrodes provide a better current-injection contact with MgO than Pt or Rh electrodes.

G. Impurity effects

1. Characteristic times for breakdown

The flow of current under a given experimental condition is qualitatively similar for all the MgO crystals, but the characteristic time for breakdown depends strongly on both the impurity and its concentration. An undoped MgO crystal typically required 22 h for the current to reach 18 mA. Crystals doped with V, Cr, Fe, or Ni had lower characteristic times for breakdown and, therefore, were more susceptible to breakdown. However, it has been found that doping with H, Co, or Cu increases the time required for dielectric breakdown.[29] The data are illustrated in Fig. 13 and shown in Table II. Clearly, impurities play an important role in determining the lifetime of MgO crystals used as electrical insulators at high temperatures. For example, the characteristic time for breakdown of MgO doped with 30 ppm Cu is 20 times longer than that of the undoped crystals under the same conditions. The characteristic time for breakdown is determined not only by the dopant but also by its concentration. This observation has been reported elsewhere.[29]

2. Activation energy

The activation energy associated with the breakdown of MgO crystals was computed from three different measurements: the time constant τ_2, the short-circuit current I_{SC}, and the alternating current I_{ac}.[27] The activation energies obtained from doped and undoped MgO crystals range from 2.1 to 2.8 eV, as shown in Table III. Using the values of either τ_2 or I_{SC}, the same activation energy is calculated for each sample; the method of I_{ac} also yields the same activation energy, except for the Cu- and Co-doped MgO crystals, in which lower activation energies are determined from either τ_2 or I_{SC}. It has been found that a lower activation energy results in a longer characteristic time for breakdown, and vice versa. This correlation has also been found to be true in MgO:Ni crystals with different dopant levels, as shown in Tables II and III.

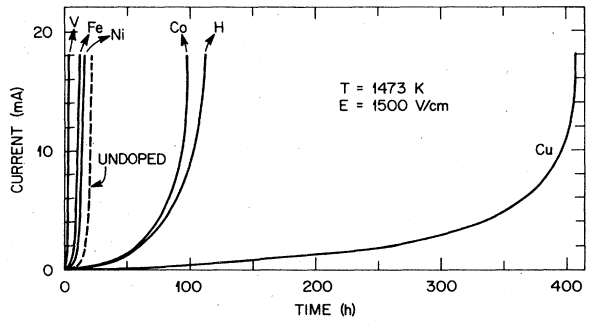

FIG. 13. Current vs time at $T=1473$ K with $E=1500$ V/cm applied to doped and undoped MgO crystals. Crystals doped with V, Fe, or Ni have a lower characteristic time for breakdown than the undoped one, but the crystals doped with Co, H, or Cu have higher characteristic times for breakdown.

TABLE II. Characteristic times for the breakdown of MgO crystals at 1473 K and 1500 V/cm. Column 3 corresponds to the concentration of dopants tabulated in column 1. Column 4 lists the characteristic times for breakdown (in the first cycle).

Sample	Source	n (ppm)	t_c (h)
MgO	ORNL	<100[a]	22
MgO:Ni	ORNL	4280	16
	ORNL	1000	1
MgO:Fe	Tateho	1000	12
MgO:Co	ORNL	2080	95
MgO:Cu	ORNL	30	406
MgO:V	Tateho	350	3
MgO:Cr	Tateho	720	1
MgO:H	ORNL		110

[a]Total impurity.

IV. SUMMARY AND CONCLUSION

The study of the dielectric breakdown of MgO crystals at elevated temperatures is extended to include the effects of some important parameters, such as temperature, geometry, electric field, atmospheric condition, electrode material, and dopant impurity. Each parameter is investigated individually. The results are summarized as follows:

(1) The time-dependent current decreases initially to a

TABLE III. Activation energies for the breakdown of MgO crystals. Activation energies shown were computed from three measurements: short-circuit current I_{SC}, time constant τ_2, and alternating current I_{ac}.

		Activation energy (eV)		
Sample	n (ppm)	I_{SC}	τ_2	I_{ac}
MgO	<100[a]	2.4[b]	2.3	2.4
MgO:Ni	4280	2.4	2.3	2.4
	1000	2.6		
MgO:Fe	1000	2.8	2.7	2.7
MgO:Co	2080	2.2	2.1	2.6
MgO:Cu	30	2.2[b]	2.1	2.7
MgO:V	350	2.7	2.7	2.7
MgO:Cr	720	2.6	2.6	
MgO:H		2.6		2.5

[a]Total impurity.
[b]Values of I_{SC} are small compared with the background noise and the results are only estimated.

minimum before increasing, and can be described as a sum of two exponentials with two different time constants τ_1 and τ_2 [Eq. (1)]. τ_1 is responsible for the decrease of the current and τ_2 describes the current increase and hence the breakdown. The time constant τ_2, which is directly related to the breakdown time, has an exponential dependence on temperature and dc electric field strength, as described in Eq. (4).

(2) An alternating electric field with a frequency of 60 Hz cannot cause breakdown. This fact leads to the conclusion that the mechanism leading to breakdown is not due to thermal effects, and lends support to the double-injection model.

(3) The dielectric breakdown time of MgO crystals, under the experimental conditions of $T=1473$ K and $E=1500$ V/cm, is essentially independent of the sample thickness. This fact indicates that, if the migration of ionic species or vacancies is directly involved in the breakdown process, the migration is short ranged.

(4) The characteristic time for breakdown of MgO crystals in air is twice that in either pure oxygen or pure nitrogen.

(5) Electrode materials can greatly affect the current behavior and therefore the breakdown characteristics. Iridium electrodes provide a rapid current increase and hence cause a breakdown much faster than Pt or Rh electrodes. This phenomenon indicates that Ir provides better current injection in MgO.

(6) The breakdown characteristics are also determined by impurities and their concentrations. Some of the impurities, such as Cr, V, Ni, and Fe, cause more rapid breakdown. Others, such as H, Co, and Cu, slow the breakdown process and prolong the lifetime of MgO crystals used as electrical insulators. The enhancement or suppression of breakdown in MgO are determined by the impurity concentration.[27]

(7) Potential-profile measurements show that the electric field normal to the electrodes tends toward a constant value as the current increases. This behavior demonstrates that local electrical neutrality prevails at higher currents and also that breakdown is not due to polarization.

(8) Activation energies can be obtained by measuring the temperature dependence of the time constant τ_2 or the short-circuit current I_{SC}. These two measurements identify the same mechanism for the conduction process.[42]

The current conduction as well as the breakdown can be satisfactorily described by a double-injection model involving drift of ionic species or vacancies.[27,42] The current increase results from an increase in hole injection, which is enhanced by the migration of negatively charged ionic species or vacancies towards the anode, as well as the development of local electrical neutrality. The time constant τ_2 [Eq. (1)] appears to be related to the short-range migration of the negatively charged ionic species or vacancies towards the anode, and the nearly constant short-circuit current (at $t > 10$ min) suggests relaxation of the accumulated carriers. This mechanism is supported by the experimental fact that the same activation energy is always obtained from the temperature dependence of the time constant τ_2 or the short-circuit current I_{SC}. Evidence for local electrical neutrality is provided by the potential profiles (Figs. 6 and 8). However, our data on the potential profiles are inadequate to describe the details of potential distribution in the regions near the electrodes. Such information would be useful to verify the double-injection model. Impurities are expected to directly affect the current behavior and the breakdown characteristics, because impurities can either create charge-trapping sites which affect the development of the local electrical neutrality, or create vacancies (or ionic species) which determine the rate of increase of hole injection.

ACKNOWLEDGMENT

One of us (K.L.T.) is grateful for the hospitality of members of the Solid State Division during his stay at ORNL. This research was sponsored by the Division of Materials Sciences, U.S. Department of Energy, under Contract No. W-7405-eng-26 with the Union Carbide Corporation.

[1]J. H. Calderwood and R. Cooper, Proc. Phys. Soc. London, Sect. B **66**, 74 (1953).
[2]R. Cooper, D. T. Grossard, and A. A. Wallace, Proc. Phys. Soc. London, Sect. B **70**, 169 (1957).
[3]R. Cooper, R. M. Higgin, and W. A. Smith, Proc. Phys. Soc. London, Sect. B **76**, 817 (1960).
[4]R. Cooper and D. L. Pulfrey, J. Phys. D **4**, 292 (1971).
[5]R. Cooper and W. A. Smith, Proc. Phys. Soc. London, Sect. B **78**, 734 (1961).
[6]J. R. Hanscomb, Aust. J. Phys. **15**, 504 (1962).
[7]J. R. Hanscomb, J. Phys. D **2**, 1327 (1969).
[8]J. R. Hanscomb, J. Appl. Phys. **41**, 3597 (1970).
[9]J. R. Hanscomb, K. C. Kao, J. H. Calderwood, J. J. O'Dwyer, and P. R. Emtage, Proc. Phys. Soc. London **88**, 425 (1966).
[10]L. R. Schissler, Massachusetts Institute of Technology, Technical Report No. 153 (1960) (unpublished).
[11]D. B. Watson, K. C. Kao, and J. H. Calderwood, IEEE Trans. Electron. Insul. **EL-1**, 30 (1965).
[12]D. B. Watson and W. Heyes, J. Phys. Chem. Solids **31**, 1531 (1970).
[13]R. C. Merrill and R. A. West, J. Electrochem. Soc. **110**, 49C (1963).
[14]P. P. Budenstein, P. J. Hayes, J. L. Smith, and W. B. Smith, J. Vac. Sci. Technol. **6**, 289 (1969).
[15]P. R. Emtage and J. J. O'Dwyer, Phys. Rev. **16**, 356 (1966).
[16]F. Forlani and N. Minnaja, Phys. Status Solidi **4**, 311 (1964).
[17]H. Frolich, Proc. R. Soc. London Ser. A **188**, 521 (1947).
[18]H. Frolich and B. V. Paranjape, Proc. Phys. Soc. London, Sect. B **69**, 21 (1956).
[19]T. E. Hartman and J. S. Chivian, Phys. Rev. **134**, A1094 (1964).
[20]W. D. Kingery, H. K. Bowen, and D. R. Uhlman, *Introduction to Ceramics*, 2nd ed. (Wiley, New York, 1976).
[21]D. R. Lamb, *Electrical Conduction Mechanisms in Thin Insulating Films* (Methuen, London, 1967).
[22]M. Lenzlinger and E. H. Snow, J. Appl. Phys. **40**, 2788 (1969).
[23]S. Whitehead, *Dielectric Breakdown of Solids* (Oxford University Press, Oxford, 1951).
[24]R. Stratton, Progr. Dielectr. **3**, 235 (1961).
[25]J. J. O'Dwyer, J. Phys. Chem. Solids **28**, 1137 (1967).

[26]J. J. O'Dwyer, *The Theory of Electrical Conduction and Breakdown in Solid Dielectrics* (Oxford University Press, Oxford, 1973).
[27]K. L. Tsang, Y. Chen, and J. J. O'Dwyer, Phys. Rev. B **26**, 6909 (1982).
[28]K. L. Tsang, Ph.D. thesis, University of Alabama, Birmingham, 1983.
[29]K. L. Tsang and Y. Chen, J. Appl. Phys. **54**, 4531 (1983).
[30]E. Sonder, K. F. Kelton, J. C. Pigg, and R. A. Weeks, J. Appl. Phys. **49**, 5971 (1978).
[31]J. Narayan, R. A. Weeks, and E. Sonder, J. Appl. Phys. **49**, 5977 (1978).
[32]F. A. Modine, L. A. Boatner, M. M. Abraham, W. P. Unruh, and R. Bunch, Bull. Am. Phys. Soc. **24**, 413 (1979).
[33]R. A. Weeks, J. Narayan, and E. Sonder, Phys. Status Solidi A **70**, 631 (1982).
[34]M. M. Abraham, C. T. Butler, and Y. Chen, J. Chem. Phys. **55**, 3752 (1971).
[35]A. J. Moulson, W. R. Phillips, and P. Popper, in *Special Ceramics,* edited by P. Popper (Academic, London, 1965), p. 199.
[36]J. Cohen, J. Phys. Chem. Solids **16**, 285 (1960).
[37]M. A. Lampert and P. Mark, *Current Injection in Solids* (Academic, New York, 1970).
[38]T. J. Lewis and A. J. Wright, J. Appl. Phys. D **1**, 441 (1968).
[39]T. J. Lewis and A. J. Wright, J. Appl. Phys. D **3**, 1329 (1970).
[40]H. Inouye, C. T. Liu, and R. G. Donnelly, Oak Ridge National Laboratory Report No. ORNL-4813,19 (1972) (unpublished).
[41]C. T. Liu and H. Inouye, Oak Ridge National Laboratory Report No. ORNL-5240,30 (1976) (unpublished).
[42]K. L. Tsang, H. T. Tohver, and Y. Chen, in *Defect Properties and Processing of High-Technology Nonmetallic Materials,* Vol. 24 of *Materials Research Society Symposium Proceedings,* edited by J. H. Crawford, Jr., Y. Chen, and W. A. Sibley (North-Holland, New York, 1984), p. 207.